Fluid Phase Equilibria 407 (2016) 236–242

Contents lists available at ScienceDirect

Fluid Phase Equilibria

journal homepage: www.elsevier.com/locate/fluid

Molecular dynamics simulations of the diffusion coefficients of light *n*-alkanes in water over a wide range of temperature and pressure

Vasileios K. Michalis[a], Othonas A. Moultos[a], Ioannis N. Tsimpanogiannis[a,b], Ioannis G. Economou[a,*]

[a] Chemical Engineering Program, Texas A&M University at Qatar, P.O. Box 23847, Doha, Qatar
[b] Environmental Research Laboratory, National Center for Scientific Research "Demokritos", 15310 Aghia Paraskevi Attikis, Greece

ARTICLE INFO

Article history:
Received 22 March 2015
Received in revised form 27 May 2015
Accepted 30 May 2015
Available online 3 June 2015

Keywords:
Diffusion coefficient
n-alkanes
Paraffin
H_2O
Molecular dynamics
Simulations

ABSTRACT

The diffusion coefficients of the first five *n*-alkanes in water at infinite dilution have been obtained from molecular dynamics simulations over a wide range of temperatures at 0.1 MPa and additionally, for methane and *n*-butane, at higher pressures up to 200 MPa. Comparison with available experimental data provides confidence in the accuracy of the predictions using the TIP4P/2005 model for water and the TraPPE force field for *n*-alkanes. Additionally, a Speedy–Angell-type phenomenological equation that captures the pressure and temperature behavior of the methane and *n*-butane is provided which can be used for engineering calculations. Furthermore, it is shown that the diffusion coefficients of methane and *n*-butane obey the Stokes–Einstein equation. Finally, the molecular structure of water–*n*-alkane mixtures is examined.

1. Introduction

Diffusion coefficients of the binary mixtures of water (H_2O) with light hydrocarbons are important for the study and design of numerous geological [1], petroleum [2–4] and chemical [5,6] engineering and environmental [7] applications. Light hydrocarbons are produced massively in the subsurface [8] either biogenically [9,10] or thermogenically [8], depending on the prevailing temperature and pressure conditions. Upon accumulation they can migrate upwards, as a result of buoyancy forces. If interstitial H_2O is encountered by the light *n*-alkanes, either during the production or the migration stages, dissolution and subsequent diffusion will take place. In oceanic sediments the migrating gases can encounter the hydrate stability zone (provided that the pressure and temperature conditions are appropriate), where they can remain trapped in the form of solid clathrate hydrates [11]. If hydrate formation is not possible, eventually the migrating gas can reach the ocean floor. The competition between advection and diffusion in the H_2O column will determine whether the light *n*-alkanes will eventually escape to the atmosphere [12]. Such processes can have a significant effect to the global climate since methane (CH_4) is a strong greenhouse gas.

The diffusion coefficients of short *n*-alkane molecules in H_2O for temperatures up to approximately 400 K and atmospheric pressures have been repeatedly measured experimentally during the last 5 decades [13–21]. More recently, the diffusion coefficients of CH_4 in H_2O for temperatures up to 473 K and pressures up to 40 MPa have been measured by Guo et al. [22] by means of Raman spectroscopy. The authors proposed a Speedy–Angell power-law-type [23] correlation for the calculation of the diffusion coefficient of infinite diluted CH_4 in H_2O. Mutoru et al. [24] correlated the available experimental results and proposed a novel phenomenological model for the prediction of the mutual diffusion coefficients of the H_2O–CO_2 mixture, that performs equally well for binary mixtures of H_2O with light *n*-alkanes (CH_4, C_2H_6 and C_3H_8). A thorough discussion of various semi-empirical correlations, based either on the kinetic theory of Chapman–Enskog [25,26] or on the Stokes–Einstein hydrodynamic theory [27], is reported by Cussler [28], and Taylor and Krishna [29].

The experimental determination of thermodynamic properties and transport coefficients is usually costly and difficult to perform, especially when measurements at high pressures and/or temperatures are required. Alternative approaches like atomistic simulations have been proven reliable techniques for estimating thermodynamic or transport properties at temperature and

* Corresponding author.
E-mail address: ioannis.economou@qatar.tamu.edu (I.G. Economou).

http://dx.doi.org/10.1016/j.fluid.2015.05.050
0378-3812/

pressure conditions that are experimentally unfeasible. To this purpose, various simple, yet efficient force-fields, for the representation of H_2O (as is discussed in detail in the reviews [30,31]), and *n*-alkane [32–35] molecules were developed.

Despite the significant effort that was put into the prediction of phase equilibria of mixtures of H_2O with *n*-alkanes [36–44] by many research groups, only one molecular simulation study exists in the literature for the diffusion coefficient of CH_4 in H_2O, while none for higher *n*-alkanes. Specifically, Shvab and Sadus [45] have performed an extensive series of molecular dynamics (MD) simulations for the calculation of a number of thermodynamic properties and diffusion coefficients of the H_2O–CH_4 mixture for various CH_4 compositions. The authors reported extended calculations that include the pressure–temperature behavior, isothermal and adiabatic compressibility, thermal pressure and expansion coefficients, heat capacity, speed of sound, and Joule–Thomson and diffusion coefficients.

From the above, it becomes clear that a comprehensive study of the diffusion coefficients of short *n*-alkane molecules in H_2O over the range of temperatures and pressures relevant to industrial and geological applications is still needed. The main objective of the current study is to report an extensive series of MD simulations for the diffusion coefficients of CH_4, C_2H_6, C_3H_8, *n*-C_4H_{10}, and *n*-C_5H_{12} in H_2O at a wide range of temperatures (up to 623.15 K) and pressures (up to 200 MPa). The structure of this paper is as follows: In Section 2, a short description of the intermolecular potentials and the simulation methods used is given. In Section 3, a brief analysis of the molecular structure of H_2O–*n*-alkane mixtures is presented followed by presentation of the results for the diffusion coefficient and a comparison with the available experimental data, that are limited to pressures up to 40 MPa for the case of H_2O–CH_4, and to 0.1 MPa for all the other mixtures considered in the current study. Additionally, we present a phenomenological model for the calculation of the diffusivities of *n*-alkanes in H_2O as a function of pressure and temperature, which can be used for engineering calculations. Finally, we conclude with a brief summary of our findings.

2. Model and methods

2.1. Intermolecular potentials

For the representation of H_2O the TIP4P/2005 [46] force field was used. The TIP4P/2005 is a rigid 4-site model in which a Lennard–Jones (LJ) sphere is fixed on the oxygen site. The electrostatic contributions are implemented by positive partial charges located on each hydrogen atom and a negative partial charge fixed on an "M-site", located on the bisector of the H–O–H angle at 0.1546 Å from the oxygen atom. For the *n*-alkanes, the TraPPE [32] model was employed. Since the TraPPE force field is based on a united atom (UA) description, different pseudoatoms are used to describe CH_4, CH_3 and CH_2 groups. The non-bonded interactions between the pseudoatoms separated by more than three bonds or belonging to different molecules were calculated by the LJ potential:

$$U^{\mathrm{LJ}}(r_{ij}) = 4\varepsilon_{ij}\left[\left(\frac{\sigma_{ij}}{r_{ij}}\right)^{12} - \left(\frac{\sigma_{ij}}{r_{ij}}\right)^{6}\right] \tag{1}$$

where ε_{ij}, σ_{ij}, and r_{ij} are the LJ well depth, the LJ size, and the distance for the atoms i and j, respectively. The non-bonded interactions between H_2O molecules were calculated as the sum of the LJ repulsion–dispersion and the Coulombic interactions:

$$U^{\mathrm{coul}}(r_{ij}) = \frac{q_i q_j}{4\pi\varepsilon_0 r_{ij}} \tag{2}$$

where ε_0 is the vacuum permittivity.

The LJ parameters for the interactions between atoms belonging to different molecules were calculated using the standard Lorenz–Berthelot combining rules [47]:

$$\varepsilon_{ij} = \left(\varepsilon_{ii}\varepsilon_{jj}\right)^{1/2} \tag{3}$$

$$\sigma_{ij} = \frac{1}{2}(\sigma_{ii} + \sigma_{jj}) \tag{4}$$

In all cases studied, the pseudoatoms are connected by bonds with a fixed length and the bond angle bending is given by a harmonic potential:

$$U^{\mathrm{bend}}(\theta) = \frac{k_\theta}{2}(\theta - \theta_0)^2 \tag{5}$$

where k_θ and θ_0 are the force constant [48] and the equilibrium angle, respectively. The 1–4 bonded interactions are described by the OPLS united atom torsional potential [35]:

$$U^{\mathrm{tors}}(\phi) = c_0 + c_1[1 + \cos\phi] + c_2[1 - \cos 2\phi] + c_3[1 + \cos 3\phi] \tag{6}$$

where ϕ is the dihedral angle and c_i are constants. The values of the parameters of the force fields used in the present study are listed in Table 1.

2.2. Computational details

MD simulations were performed in the isothermal–isobaric (NPT) ensemble using the GROMACS open-source molecular simulation platform (version 4.6.5) [49,50]. A cubic box with periodic boundary conditions in all directions was used. The leap-frog integration scheme was used with a time step of 1 fs, while the temperature and pressure were maintained constant using the Nosé–Hoover [51,52] and Parrinello–Rahman [53] methods respectively. The coupling constants of the thermostat and barostat were set to 1 ps. Long-range Coulombic interactions were handled using the particle mesh Ewald (PME) method [54,55]. The cut-off distance was set to 14 Å, both for the LJ potential and the real space components of the PME summations, while tail corrections were applied for energy and pressure.

An equilibration period of 5 ns was carried out for each system examined, prior to any diffusion coefficient calculations. Subsequently, for each system, 25 production runs 2 ns long were performed. Monitoring the energy, pressure, and temperature during the production period showed that they were well stabilized, with small fluctuations present, typical for any MD simulation. The molecular trajectories were sampled every

Table 1
Force-field parameters for H_2O and *n*-alkanes examined in this study. The parameters between unlike atoms were calculated by the combining rules of Eqs. (3) and (4). Methyl (CH_3) and methylene (CH_2) pseudoatom parameters are common in C_2H_6, C_3H_8,*n*-C_4H_{10}, and *n*-C_5H_{12}. k_B is the Boltzmann constant.

TIP4P/2005		TraPPE	
H–O–H (°)	104.52	$l_{C\text{-}C}$ (Å)	1.54
$l_{O\text{-}H}$ (Å)	0.9572	θ_0(°)	114
$\sigma_{O\text{-}O}$ (Å)	3.1589	σ_{CH_4} (Å)	3.73
$\sigma_{H\text{-}H}$ (Å)	0	σ_{CH_3} (Å)	3.75
$\varepsilon_{O\text{-}O}/k_B$ (K)	93.2	σ_{CH_2} (Å)	3.95
$\varepsilon_{H\text{-}H}/k_B$ (K)	0	ε_{CH_4}/k_B(K)	148
q_O (e)	−1.1128	ε_{CH_3}/k_B(K)	98
q_H (e)	0.5564	ε_{CH_2}/k_B(K)	46
		k_θ/k_B (K/rad^2)	62,500
		c_0/k_B (K)	0
		c_1/k_B (K)	355.03
		c_2/k_B (K)	−68.19
		c_3/k_B (K)	791.32

1000 steps, resulting in a total of 2000 configurations per run, from which diffusion coefficients were calculated.

The diffusion coefficients, D, were calculated using the Einstein relation, according to which D is obtained from the solute mean square displacement [47,56]:

$$D = \lim_{t\to\infty} \frac{\left\langle \frac{1}{N}\sum_{i=1}^{N} [r_i(t) - r_i(0)]^2 \right\rangle}{6t} \quad (7)$$

where $r_i(t)$ is the unfolded position of the center of mass of the solute at time t, and the angle brackets indicate an ensemble average over all solute molecules and time origins. In order to improve the statistics of our results, the diffusion coefficient for each state point was calculated by averaging the results of 25 independent simulations, each one starting from a different initial configuration, thus leading to a wide divergence of the trajectories of the molecules.

The number of solvent molecules in the majority of production runs was 2000 and the number of solute molecules was 10, resulting in a mole fraction for solute equal to 5×10^{-3}, which corresponds to near infinite dilution conditions. It should be mentioned that this composition is above the solubility of the n-alkanes in H_2O. Such a number of solute molecules reduced the statistical uncertainty (see Fig. 1), while no clustering was observed. The only exception was made for the case of n-C_5H_{12} in H_2O for which one solute molecule was used, as clustering was observed for higher composition values.

In order to verify that the results are independent of the number of solute molecules in the low composition regime examined, MD simulations with different number of solute molecules were performed. In Fig. 1, the diffusion coefficients of 1, 5 and 10 solute molecules (for the cases of CH_4, C_2H_6, C_3H_8, and n-C_4H_{10}) in 2000 H_2O molecules at 0.1 MPa and 353.15 K are shown. In all cases, the mean values of diffusion coefficients remain practically constant. On the other hand, the statistical uncertainties decrease from approximately 25% for the case of one solute molecule to 5% for the case of 10 solute molecules. Additionally, according to recent studies [57–59], such a large number of solvent molecules is expected to mitigate any system-size effects in the simulations.

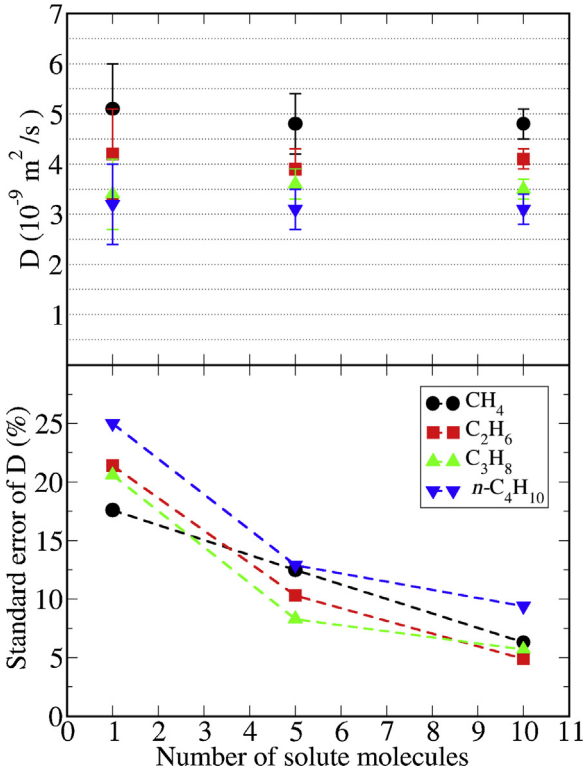

Fig. 1. (top) MD calculations for the diffusion coefficients of n-alkanes in H_2O and (bottom) standard deviation of diffusion coefficients as a function of solute number of molecules, at 353.15 K and 0.1 MPa.

The solute diffusion coefficient is related to the solvent viscosity. The Stokes–Einstein equation provides a theoretical justification of this relation, as discussed in the Section 3. Accordingly, it is important to ensure that the force field for H_2O (TIP4P/2005) predicts accurately the viscosity over the range of conditions examined. A series of MD simulations were performed to calculate of the viscosity using the Green–Kubo relation:

$$\eta(t) = \frac{V}{K_B T}\int_0^t \langle P_{\alpha\beta}(t_0) P_{\alpha\beta}(t_0 + t)\rangle dt \quad (8)$$

where V is the volume of the simulation box and $P_{\alpha\beta}$ denotes the off-diagonal element of the pressure tensor. The angle brackets indicate an ensemble average over all time origins. In order to reduce statistical uncertainty, we averaged the autocorrelation functions over all independent off-diagonal tensor elements P_{xy}, P_{xz}, P_{yz}; because of rotational invariance we also added the equivalent $(P_{xx} - P_{yy})/2$ and $(P_{yy} - P_{zz})/2$ terms. Viscosity at each state point was calculated from 10 independent simulations performed in the canonical (NVT) ensemble, using 1000 H_2O molecules. Each run was 10 ns long, while the pressure tensor elements were sampled every time step. All other simulation details are the same as described above, for the calculation of diffusion coefficients. The MD results for the H_2O viscosity are shown in Fig. 2 and are compared with the viscosity values from the NIST database [60] which practically coincide with the experimental data. Excellent agreement between NIST data and simulation results is observed. Each run was executed in 32 cores, with Intel Xeon 2.7 GHz processors, and needed about 10 wall-clock hours to be completed.

3. Results and discussion

3.1. Microscopic structure of H_2O–n-alkane mixtures

The radial distribution function, $g(r)$, between H_2O and n-alkane molecules at 298.15 K and 0.1 MPa calculated from MD simulations is shown in Fig. 3. For the case of H_2O–CH_4, there is a first strong peak at approx. 0.37 nm with a height of 2.04. The corresponding first peak for H_2O–H_2O interactions has a height of 3.26 (not shown

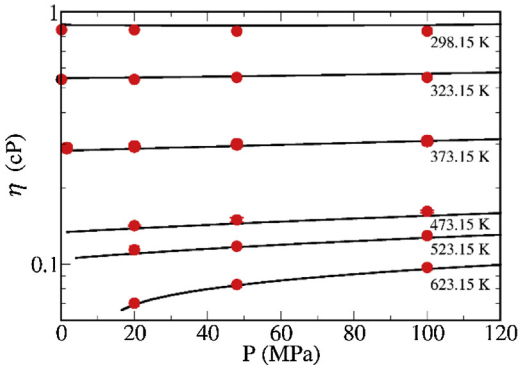

Fig. 2. Viscosity of H_2O as a function of pressure at various temperatures. Black solid lines correspond to values from the NIST database [60]. Red circles correspond to TIP4P/2005 model. The error bars are smaller than the symbol size. (For interpretation of the references to color in this figure legend, the reader is referred to the web version of this article.)

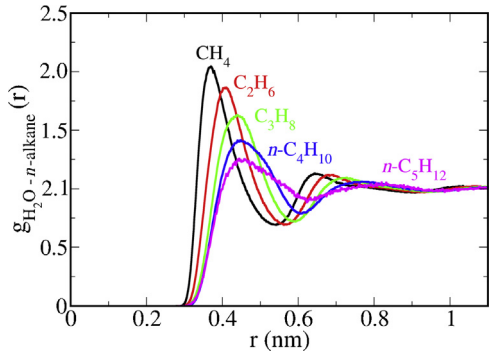

Fig. 3. Radial distribution function for H_2O–*n*-alkanes at 298.15 K and 0.1 MPa from MD simulations.

here), due to strong hydrogen bonding. The position of the first peak shifts progressively to longer distances as the *n*-alkane size increases reaching a value of 0.45 nm for *n*-C_5H_{12} with a simultaneous decrease of the peak height and increase of the peak width. This is due to the increase of the molecular size of the *n*-alkanes that results in positioning solvent molecules at longer distances. A similar behavior is observed for the second peak as well.

For *n*-C_4H_{10} and larger *n*-alkanes, the distribution of torsional angles provides a quantitative description of the molecular conformations. In Fig. 4, the normalized torsional angle distribution for *n*-C_5H_{10} at 298.15 K and 0.1 MPa is shown. For comparison, the same quantity for the case of pure *n*-C_5H_{10} is presented. The two distributions are practically identical which manifests that the conformation of the relative short *n*-alkanes does not change when dissolved in H_2O. This behavior changes progressively for longer *n*-alkanes.

3.2. Temperature dependence of the diffusion coefficients and comparison with experiments

In order to validate our simulation results for the diffusion coefficient of *n*-alkanes, we performed a comparison with the available experimental data. For all the *n*-alkanes studied, with the exception of CH_4, there are experimental data only at 0.1 MPa [13–17,24]. For the case of CH_4, Guo et al. [22] reported diffusion coefficient values for temperatures up to 473 K and for pressures up to 40 MPa. In Fig. 5, Tables 2 and 3 the diffusion coefficient of CH_4 in H_2O is presented as a function of temperature at 0.1 MPa, 5 MPa, and 20 MPa, and is compared with the available experimental data [13–17,22,24]. In Fig. 6, the diffusion coefficients of

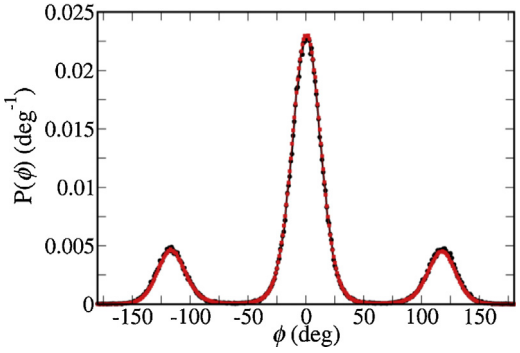

Fig. 4. Normalized probability distribution of the torsional angles of pure *n*-C_5H_{12} (black) and of *n*-C_5H_{12} in H_2O (red) at 298.15 K and 0.1 MPa. (For interpretation of the references to color in this figure legend, the reader is referred to the web version of this article.)

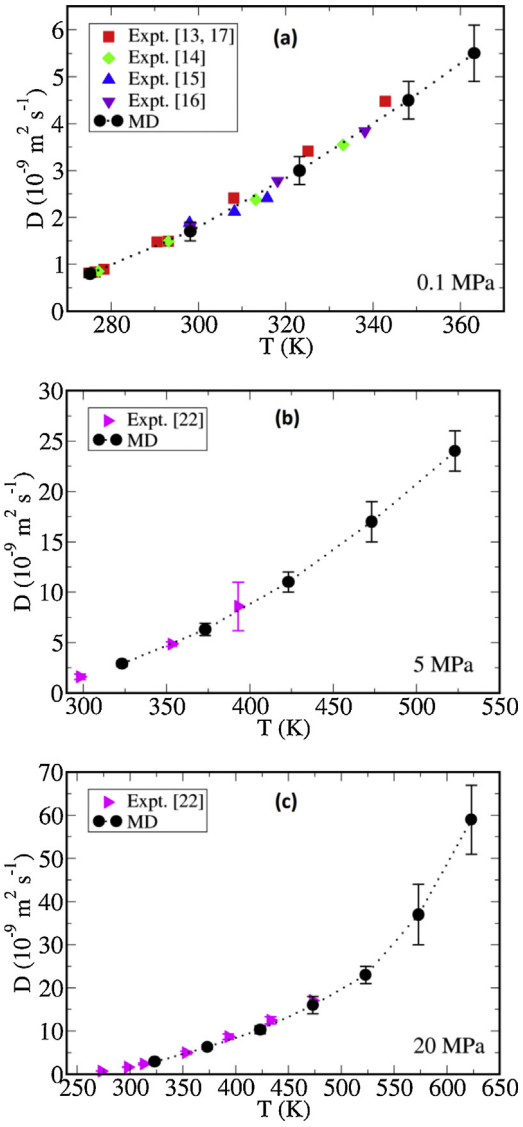

Fig. 5. Diffusion coefficient of CH_4 in H_2O at (a) 0.1 MPa, (b) 5 MPa and (c) 20 MPa. The dotted line connecting the MD results is to guide the eye.

Table 2
Diffusion coefficient of *n*-alkanes in H_2O at 0.1 MPa.

T (K)	Diffusion coefficient (10^{-9} m^2/s)				
	CH_4	C_2H_6	C_3H_8	*n*-C_4H_{10}	*n*-C_5H_{12}
275.15	0.80 ± 0.08	0.60 ± 0.05	0.54 ± 0.06	0.49 ± 0.05	0.5 ± 0.1
298.15	1.7 ± 0.2	1.3 ± 0.1	1.1 ± 0.1	1.07 ± 0.09	1.0 ± 0.3
323.15	3.0 ± 0.3	2.4 ± 0.2	2.1 ± 0.2	1.9 ± 0.2	1.7 ± 0.4
348.15	4.5 ± 0.4	3.7 ± 0.4	3.1 ± 0.3	3.0 ± 0.3	2.6 ± 0.6
363.15	5.5 ± 0.6	4.6 ± 0.3	4.0 ± 0.4	3.8 ± 0.5	3.3 ± 0.7

C_2H_6, C_3H_8, *n*-C_4H_{10}, and *n*-C_5H_{12} in H_2O are shown along with the respective experimental values [14,15] at 0.1 MPa, for the temperature range 274.9–333.15 K.

In all cases, the diffusion coefficients increase with temperature, which is typical for gases dissolved in liquids [28,29]. From Figs. 5 and 6, it can be seen that the combination of TIP4P/2005–TraPPE models provides an excellent agreement between the simulation results and the experiments for all the systems and conditions examined.

Table 3
Diffusion coefficient of CH_4 and n-C_4H_{10} in H_2O at elevated pressures.

T (K)	P (MPa)	Diffusion coefficient (10^{-9} m^2/s)	
		CH_4	n-C_4H_{10}
323.15	5	2.9 ± 0.3	1.9 ± 0.2
	20	2.9 ± 0.3	1.9 ± 0.2
	50	2.7 ± 0.3	1.8 ± 0.2
	100	2.7 ± 0.3	1.8 ± 0.2
	200	2.4 ± 0.3	1.6 ± 0.2
373.15	5	6.3 ± 0.6	4.1 ± 0.4
	20	6.3 ± 0.5	4.0 ± 0.4
	50	6.0 ± 0.6	3.9 ± 0.3
	100	5.4 ± 0.5	3.6 ± 0.4
	200	5.0 ± 0.4	3.3 ± 0.3
423.15	5	11 ± 1	7.1 ± 0.8
	20	10.3 ± 0.9	6.8 ± 0.7
	50	10 ± 1	6.3 ± 0.7
	100	8.8 ± 0.9	6.2 ± 0.6
	200	7.8 ± 0.6	5.3 ± 0.5
473.15	5	17 ± 2	11 ± 1
	20	16 ± 2	10.4 ± 0.9
	50	15 ± 2	10 ± 0.9
	100	13 ± 1	8.9 ± 0.8
	200	11.6 ± 0.8	7.6 ± 0.9
523.15	5	24 ± 2	16 ± 1
	20	23 ± 2	15 ± 2
	50	21 ± 2	14 ± 2
	100	19 ± 2	13 ± 1
	200	15 ± 2	10 ± 1
573.15	20	37 ± 7	22 ± 3
	50	30 ± 3	19 ± 2
	100	25 ± 2	17 ± 2
	200	20 ± 2	14 ± 1
623.15	20	59 ± 8	37 ± 7
	50	48 ± 9	27 ± 3
	100	33 ± 4	21 ± 2
	200	25 ± 2	17 ± 2

3.3. Diffusion coefficients of CH_4 and n-C_4H_{10} in H_2O at high temperatures and pressures

Given that the combination of TIP4P/2005 with TraPPE provides an accurate prediction of the diffusion coefficients in H_2O of all hydrocarbons studied at 0.1 MPa, and particularly for CH_4 up to 20 MPa, one can expect reasonably accurate predictions at elevated conditions. Furthermore, it should be noted that the diffusion coefficient of short n-alkanes in H_2O, at infinite dilution, is strongly dependent on the density and viscosity of H_2O, two properties for which TIP4P/2005 provides excellent predictions [31,61,62].

Thus, a systematic study of the diffusion coefficients of CH_4 and n-C_4H_{10} in H_2O was performed at the temperature range 323.15–623.15 K and for pressures up to 200 MPa. The calculated diffusion coefficients are given in Table 3 and Fig. 7.

In Fig. 7(top), the diffusion coefficient of CH_4 in H_2O as a function of pressure at different temperatures is presented. It is clear that for temperatures below 473.15 K and pressures up to 50 MPa the diffusion coefficient is independent of pressure, within statistical accuracy. A similar conclusion was reached by Guo et al. [22] for pressures up to 40 MPa in their experimental investigation of the diffusion coefficient of CH_4 in H_2O. A weak dependence on pressure is observed for temperatures below 473.15 and pressures above 50 MPa. On the other hand, as the temperature increases above 473.15 K there is a pronounced effect of pressure on the diffusion coefficient for the entire pressure range considered.

A similar pressure dependence of the diffusion coefficient is found for the case of n-C_4H_{10} in H_2O, which is presented in Fig. 7(bottom). This behavior is primarily driven by the change in solvent's density, which is marginal at conditions well below the critical point but becomes substantial for high pressures and temperatures. This analysis is in line with the findings of recent experimental [63,64] and computational [57] studies for gases dissolved in H_2O.

3.4. Phenomenological model development

We used a generalized form of the Speedy–Angell (SA) equation in order to correlate the MD simulations reported in the current study, which reads as follows:

$$D^{SA}_{solute} = D_0(P)\left(\frac{T}{T_s} - 1\right)^{m(P)} \tag{9}$$

where T_s = 228 K, and the subscript solute denotes either CH_4 or n-C_4H_{10}, diffusing in H_2O, and both the parameters D_0 and m are functions of pressure P.

In order to correlate the MD results using Eq. (9), the following procedure was implemented. Initially, the MD simulations were plotted as a function of temperature. For each pressure a set of optimum values for the parameters, D_0 and m, were calculated. Subsequently, the resulting optimum parameters were correlated using the pressure as the primary variable.

For both cases of the self-diffusion coefficient of either CH_4 or n-C_4H_{10} in H_2O, it is:

$$D_0 = a_1(P) + a_2 \tag{10}$$

$$m = b_1(P) + b_2 \tag{11}$$

with the parameters: α_1, α_2, b_1, and b_2 given in Table 4 for CH_4 and n-C_4H_{10} and P is in MPa

Fig. 7 shows a comparison of the calculation of the self-diffusion coefficient of CH_4 and n-C_4H_{10} in H_2O, using Eqs. (9)–(11), with the MD simulations. We observe very good agreement for most of the pressure and temperature conditions. The only exceptions are the cases of the highest temperatures (573 and 623 K) and the lower pressures (20 MPa for 573 K, and 20 and 50 MPa for 623 K) which correspond to near critical conditions for H_2O. In these conditions, the SA equation becomes less accurate. A near critical correction to the SA could improve the agreement; however, additional parameters are needed and no further attention was given.

3.5. Stokes–Einstein analysis of the MD simulations

An analysis was performed to examine whether the MD simulations satisfy the classical Stokes–Einstein (SE) equation given by:

$$D_{SE} = \frac{k_B T}{C\pi\eta r} \tag{12}$$

where η is the viscosity of the solvent, r is the hydrodynamic radius and the C is a parameter of the drag coefficient in the analysis of the creeping flow around a sphere, that has a value of either 6 or 4 corresponding to no-slip or slip boundary conditions respectively. In the current analysis, the NIST database values for η were used [60].

By plotting D as a function of (T/η) in a logarithmic plot, as shown in Fig. 8, and performing a linear interpolation, one can calculate the slope t. For CH_4, it is t = 1.00 ± 0.02, while for n-C_4H_{10}, it is t = 1.01 ± 0.02. The calculated slopes for both cases indicate that the classical Stokes–Einstein equation is satisfied.

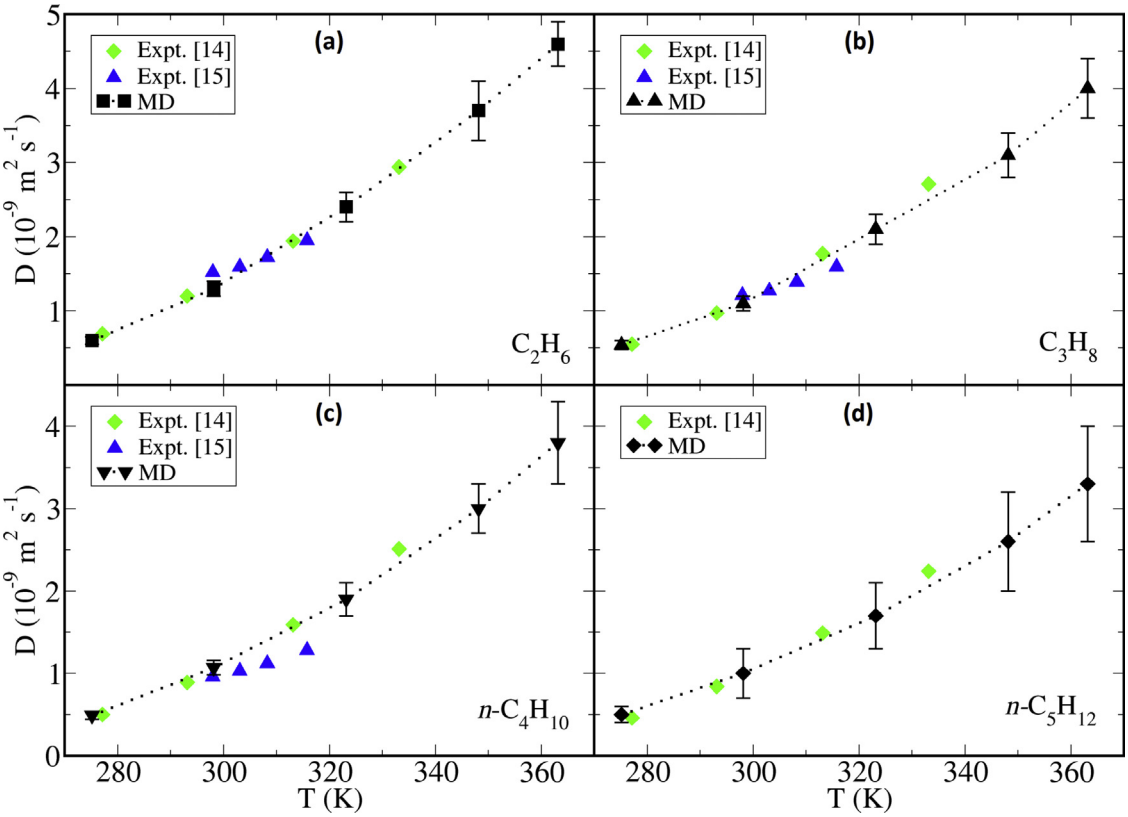

Fig. 6. Diffusion coefficient in H_2O of (a) C_2H_6, (b) C_3H_8, (c) n-C_4H_{10} and (d) n-C_5H_{12} as a function of temperature at 0.1 MPa. The dotted line connecting the MD results is to guide the eye.

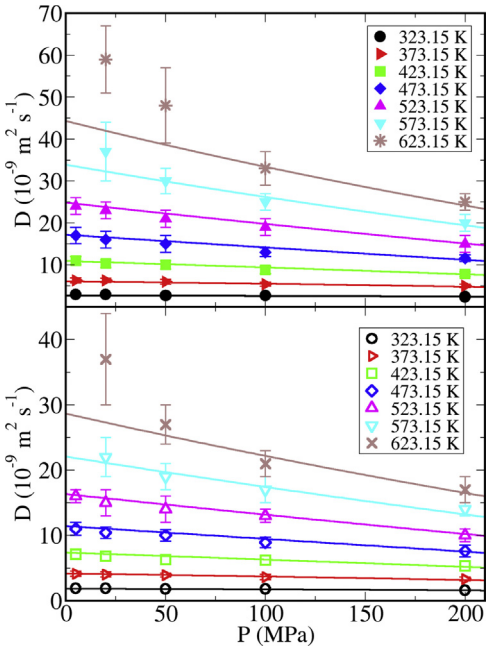

Fig. 7. Diffusion coefficient of (top) CH_4 in H_2O and (bottom) n-C_4H_{10} in H_2O as a function of pressure for various temperatures. Symbols denote the MD simulations and solid lines denote calculations using the phenomenological model of Eqs. (9)–(11).

Table 4
Parameters of Eqs. (9)–(11) for CH_4 and n-C_4H_{10}.

Parameter	CH_4	n-C_4H_{10}
α_1	-2.4638×10^{-11}	-1.6316×10^{-11}
α_2	1.4924×10^{-8}	9.9559×10^{-9}
b_1	-1.8629×10^{-3}	-1.3971×10^{-3}
b_2	1.9799	1.9233

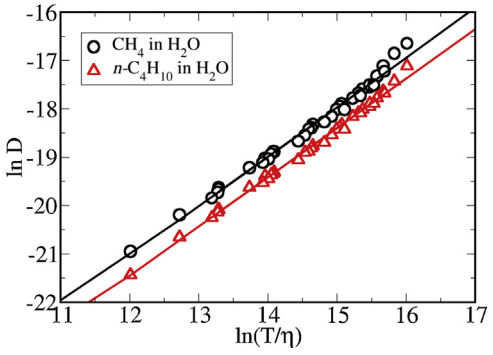

Fig. 8. $\ln(D)$ vs. $\ln(T/\eta)$ for the case of CH_4 (black circles) and n-C_4H_{10} (red triangles) diffusing in H_2O. The solid lines correspond to the best-fit lines. (For interpretation of the references to color in this figure legend, the reader is referred to the web version of this article.)

Given that the intercept of the y-axis is equal to $\ln(k_B/C\pi r)$, the hydrodynamic radius of the solute can be evaluated. The correct choice of the parameter C is, nevertheless, not obvious, because for small molecules slip boundary conditions may apply. In Fig. 9, the hydrodynamic diameter as a function of the parameter C is presented for CH_4 and n-C_4H_{10}. For the case of CH_4, the LJ diameter is 3.73 Å (dotted line). For the case of n-C_4H_{10} the hydrodynamic radius from viscosity calculations [65] is 5.34 Å (dashed-dotted line). Making the assumption that the hydrodynamic radius of CH_4

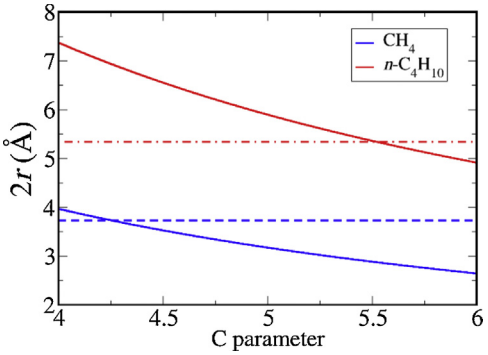

Fig. 9. Hydrodynamic diameter as a function of the C parameter of the Stokes–Einstein equation for CH_4 (blue solid line) and n-C_4H_{10} (red solid line). The dashed blue line corresponds to the LJ diameter of CH_4 and the red dashed-dotted line to the hydrodynamic diameter of n-C_4H_{10} from [65]. (For interpretation of the references to color in this figure legend, the reader is referred to the web version of this article.)

is equal to its LJ radius, a parameter C equal to 4.258 is found, which corresponds to slip boundary conditions. The respective parameter for n-C_4H_{10} turns out to be approximately 5.52 indicating a transition to no-slip boundary conditions.

4. Conclusions

The MD simulations of the diffusion coefficients for short n-alkanes using the combination of TIP4P/2005–TraPPE force field yields excellent agreement with available experimental data. For the case of CH_4 and n-C_4H_{10} it was shown that the diffusivity exhibits pressure dependence which is particularly pronounced at elevated temperature and pressure conditions. For CH_4 and n-C_4H_{10} a pressure and temperature dependent Speedy–Angel-type correlation is proposed, that can be particularly useful for fast engineering calculations. At near critical conditions for H_2O, the correlation is less accurate. Finally, it was shown that the diffusion coefficients of CH_4 and n-C_4H_{10} obey the Stokes–Einstein equation.

Acknowledgements

This publication was made possible thanks to an NPRP award [NPRP 6-1547-2-632] from the Qatar National Research Fund (a member of The Qatar Foundation). The statements made herein are solely the responsibility of the authors. We are grateful to the High Performance Computing Center of Texas A&M University at Qatar for generous resource allocation. INT is thankful to Texas A&M University at Qatar for a visiting research position.

References

[1] A. Dutkiewicz, J. Ridley, R. Buick, Chem. Geol. 194 (2003) 51–79.
[2] F. Montel, Fluid Phase Equilib. 84 (1993) 343–367.
[3] J.C. de Hemptinne, R. Peumery, V. Ruffier-Meray, G. Moracchini, J. Naiglin, B. Carpentier, J.L. Oudin, J. Connan, J. Pet. Sci. Eng. 29 (2001) 39–51.
[4] A.A. Kartsev, Geochemical Prospecting For Petroleum, 1st ed., University of California Press, 1959.
[5] K.S. Pedersen, J. Milter, C.P. Rasmussen, Fluid Phase Equilib. 189 (2001) 85–97.
[6] E.D. Sloan, C.A. Koh, Clathrate Hydrates Of Natural Gases, CRC Press, Taylor and Francis Group, 2008.
[7] S.W. Taylor, B. Sherwood Lollar, I. Wassenaar, Environ. Sci. Technol. 34 (2000) 4727–4732.
[8] G.E. Claypool, K.A. Kvenvolden, Annu. Rev. Earth Planet. Sci. 11 (1983) 299–327.
[9] D. Strąpoć, M. Mastalerz, K. Dawson, J. Macalady, A.V. Callaghan, B. Wawrik, C. Turich, M. Ashby, Annu. Rev. Earth Planet. Sci. 39 (2011) 617–656.
[10] K.-U. Hinrichs, J.M. Hayes, W. Bach, A.J. Spivack, L.R. Hmelo, N.G. Holm, C.G. Johnson, S.P. Sylva, Proc. Natl. Acad. Sci. U. S. A. 103 (2006) 14684–14689.
[11] G.D. Ginsburg, V.A. Soloviev, Mar. Geol. 137 (1997) 49–57.
[12] D.F. McGinnis, J. Greinert, Y. Artemov, S.E. Beaubien, A. Wuest, J. Geophys. Res. Oceans 111 (2006) C09007.
[13] W.J. Lu, I.M. Chou, R.C. Burruss, M.Z. Yang, Appl. Spectrosc. 60 (2006) 122–129.
[14] P.A. Witherspoon, L. Bonoli, Ind. Eng. Chem. Fund. 8 (1969) 589–591.
[15] P.A. Witherspoon, D.N. Saraf, J. Phys. Chem. 69 (1965) 3752–3755.
[16] K.E. Gubbins, K.K. Bhatia, R.D. Walker, Alche J. 12 (1966) 548–552.
[17] K.J. Sahores, P.A. Witherspoon, Advances In Organic Geochemistry, Pergamon Press, Oxford, UK, 1970.
[18] W. Sachs, J. Pet. Sci. Eng. 21 (1998) 153–164.
[19] D.M. Maharajh, J. Walkey, Can. J. Chem. 51 (1973) 944–952.
[20] B. Jahne, G. Heinz, W. Dietrich, J. Geophys. Res. 92 (1987) 10767–10776.
[21] W.S. Price, O. Söderman, J. Phys. Chem. A 104 (2000) 5892–5894.
[22] H. Guo, Y. Chen, W. Lu, L. Li, M. Wang, Fluid Phase Equilib. 360 (2013) 274–278.
[23] R.J. Speedy, C.A. Angell, J. Chem. Phys. 65 (1976) 851–858.
[24] J.W. Mutoru, A. Leahy-Dios, A. Firoozabadi, Alche J. 57 (2011) 1617–1627.
[25] R.B. Bird, D.J. Klingenberg, Adv. Water Res. B 62 (2013) 238–242.
[26] R.S. Brokaw, Ind. Eng. Chem. Process Des. Dev. 8 (1969) 240–253.
[27] C.R. Wilke, P. Chang, Alche J. 1 (1955) 264–270.
[28] E.L. Cussler, Diffusion: Mass Transfer In Fluid Systems, 3rd ed., Cambridge University Press, 2009.
[29] R. Taylor, R. Krishna, Multicomponent Mass Transfer, 1st ed., Wiley-Interscience, 1993.
[30] C. Vega, J.L.F. Abascal, M.M. Conde, J.L. Aragones, Faraday Discuss. 141 (2009) 251–276.
[31] C. Vega, J.L.F. Abascal, Phys. Chem. Chem. Phys. 13 (2011) 19663–19688.
[32] M.G. Martin, J.I. Siepmann, J. Phys. Chem. B 102 (1998) 2569–2577.
[33] S. Lago, B. Garzón, S. Calero, C. Vega, J. Phys. Chem. B 101 (1997) 6763–6771.
[34] W. Paul, D.Y. Yoon, G.D. Smith, J. Chem. Phys. 103 (1995) 1702–1709.
[35] W.L. Jorgensen, J.D. Madura, C.J. Swenson, J. Am. Chem. Soc. 106 (1984) 6638–6646.
[36] W.L. Jorgensen, J. Chem. Phys. 77 (1982) 5757–5765.
[37] J.R. Errington, G.C. Boulougouris, I.G. Economou, A.Z. Panagiotopoulos, D.N. Theodorou, J. Phys. Chem. B 102 (1998) 8865–8873.
[38] G.C. Boulougouris, J.R. Errington, I.G. Economou, A.Z. Panagiotopoulos, D.N. Theodorou, J. Phys. Chem. B 104 (2000) 4958–4963.
[39] I.G. Economou, Fluid Phase Equilib. 183–184 (2001) 259–269.
[40] A.L. Ferguson, P.G. Debenedetti, A.Z. Panagiotopoulos, J. Phys. Chem. B 113 (2009) 6405–6414.
[41] D. Paschek, Z. Phys. Chem. 223 (2009) 1091–1104.
[42] E. Johansson, K. Bolton, D.N. Theodorou, D.N. Ahlström, J. Chem Phys. 126 (2007) 224902.
[43] C. McCabe, A. Galindo, P.T. Cummings, J. Phys. Chem. B 107 (2003) 12307–12314.
[44] O. Konrad, T. Lankau, J. Phys. Chem. B 109 (2005) 23596–23604.
[45] I. Shvab, R.J. Sadus, J. Chem. Phys. 140 (2014) 104505.
[46] J.L.F. Abascal, C. Vega, J. Chem. Phys. 123 (2005) 234505.
[47] M.P. Allen, D.J. Tildesley, Computer Simulation Of Liquids, Oxford University Press, 1987.
[48] P. Van der Ploeg, H.J.C. Berendsen, J. Chem. Phys. 76 (1982) 3271–3276.
[49] H.J.C. Berendsen, D. van der Spoel, R. van Drunen, Comput. Phys. Commun. 91 (1995) 43–56.
[50] E. Lindahl, B. Hess, D. van der Spoel, J. Mol. Model. 7 (2001) 306–317.
[51] S. Nosé, Mol. Phys. 52 (1984) 255–268.
[52] W.G. Hoover, Phys. Rev. A 31 (1985) 1695–1697.
[53] M. Parrinello, A. Rahman, J. Appl. Phys. 52 (1981) 7182–7190.
[54] T. Darden, D. York, L. Pedersen, J. Chem. Phys. 98 (1993) 10089–10092.
[55] U. Essmann, L. Perera, M.L. Berkowitz, T. Darden, H. Lee, L.G. Pedersen, J. Chem. Phys. 103 (1995) 8577–8593.
[56] A. Einstein, Ann. Phys. 17 (1905) 549–560.
[57] O.A. Moultos, I.N. Tsimpanogiannis, A.Z. Panagiotopoulos, I.G. Economou, J. Phys. Chem. B 118 (2014) 5532–5541.
[58] C.G. Aimoli, E.J. Maginn, C.R.A. Abreu, J. Chem. Phys. 141 (2014) 134101.
[59] O.A. Moultos, G.A. Orozco, I.N. Tsimpanogiannis, A.Z. Panagiotopoulos, I.G. Economou, Mol. Phys. (2015) , doi:http://dx.doi.org/10.1080/00268976.2015.1023224.
[60] E.W. Lemmon, M.O. McLinden, D.G. Friend, Thermophysical properties of fluid systems, in: P.J. Linstrom, W.G. Mallard (Eds.), NIST Chemistry WebBook, NIST Standard Reference Database Number 69, National Institute of Standards and Technology, Gaithersburg, MD, 2015 http://webbook.nist.gov (retrieved 30.1.15).
[61] G. Raabe, R.J. Sadus, J. Chem. Phys. 137 (2012) 104512.
[62] G. Guevara-Carrion, J. Vrabec, H. Hasse, J. Chem. Phys. 134 (2011) 074508.
[63] S.P. Cadogan, G.C. Maitland, J.P.M. Trusler, J. Chem. Eng. Data 59 (2014) 519–525.
[64] W. Lu, H. Guo, I.M. Chou, R.C. Burruss, R.C. Li, Geochim. Cosmochim. Acta 115 (2013) 183–204.
[65] L.S. Tee, S. Gotoh, W.E. Stewart, Ind. Eng. Chem. Fund. 5 (1966) 356–363.